JOURNAL OF GEOPHYSICAL RESEARCH, VOL. 114, C05004, doi:10.1029/2008JC004956, 2009

Upwelling flow dynamics in long canyons at low Rossby number

Amy F. Waterhouse,[1,2] Susan E. Allen,[1] and Alexander W. Bowie[1]

Received 11 June 2008; revised 17 January 2009; accepted 16 February 2009; published 6 May 2009.

[1] Submarine canyons, topographic features incising the continental slope, vary in both shape and size. The dynamics of short canyons have been observed and described in the field, in the laboratory, and with numerical simulations. Flow within long canyons, such as Juan de Fuca canyon, located between Vancouver Island and Washington State in the Pacific Northwest, is less well understood. Physical models of both long and short canyons have been constructed to understand the upwelling dynamics in long canyons and how upwelling changes, as compared with the dynamics of short canyons, at low Rossby number. Stratification and rotation, both important parameters in determining the dynamics in canyons, can be controlled and scaled accordingly for replication of oceanic conditions. The physical model is spun up to an initial rotation rate, and the flow is forced by increasing the rotation rate over the equivalent of several days. Flow visualization is used to determine the strength and location of upwelling, the strength and mechanisms generating vorticity, as well as the differences between the flow within the long and short canyons. The pattern of upwelling between the two canyons is significantly different in the horizontal with upwelling occurring through the canyon head in the short canyon and upwelling occurring close to the mouth along the downstream rim in the long canyon. At high Rossby number, upwelling is similar in both the long and short canyon and is driven by advection. However, as Rossby number decreases, the flow in the long canyon is more strongly affected by the strong convergence of the isobaths near the canyon than by advection alone.

Citation: Waterhouse, A. F., S. E. Allen, and A. W. Bowie (2009), Upwelling flow dynamics in long canyons at low Rossby number, *J. Geophys. Res.*, *114*, C05004, doi:10.1029/2008JC004956.

1. Introduction

[2] Submarine canyons are topographic coastal features that incise the continental shelf and are regions of locally enhanced coastal upwelling (B. M. Hickey, Coastal submarine canyons, paper presented at Aha Huliko'a Hawaiian Winter Workshop on Topographic Effects in the Ocean, University of Hawai'i at Manoa, Honolulu, Hawai'i, 1995). The unique flow dynamics and upwelling due to these topographic features have resulted in the observation of high concentrations of zooplankton around canyon heads [*Macquart-Moulin and Patriti*, 1996; *Allen et al.*, 2001] indicating that canyons are an important mechanism for coastal upwelling. Canyons vary in both shape and size. Short canyons, such as Astoria and Barkley Canyons, feature a canyon head that reaches the depth of the continental shelf well before the coast [*Hickey*, 1997; *Allen*, 2000]. Long canyons, such as Juan de Fuca, Mackenzie and Monterrey Canyons, feature a canyon head that does not reach the continental shelf depth before the coastline, and extend far into the coastal region, where the head often ends in estuaries [*Carmack and Kulikov*, 1998; *Allen*, 2000; *Kunze et al.*, 2002; Hickey, presented paper, 1995].

[3] Flow dynamics in short canyons have been well studied and documented. As geostrophic currents pass over short canyons, water is driven up the canyon because of an unbalanced pressure gradient caused by the constrictions in the topography [*Freeland and Denman*, 1982]. This effect enhances upwelling and mixing (Hickey, presented paper, 1995). As water columns on the shelf, originating upstream of the canyon, flow over top of the canyon, they stretch as a result of an increase in bottom depth downstream of the canyon rim. The water column stretching, due to conservation of potential vorticity, creates cyclonic vorticity in the flow [*Hickey*, 1997; *Allen et al.*, 2003]. The generation of cyclonic vorticity inside the canyon has also been linked to flow separation at the canyon mouth, which advects into the canyon [*Pérenne et al.*, 2001a]. The flow then turns toward the head of the canyon and is advected up onto the shelf. A cyclonic eddy, formed because of this vortex stretching, is observed in the canyon from the shelf break depth down to the deep layers inside the canyon mouth [*She and Klinck*, 2000]. The near surface flow (<100 m) is only weakly affected by the canyon [*Hickey*, 1997; *Allen et al.*, 2003]. Most upwelling processes in

[1]Department of Earth and Ocean Sciences, University of British Columbia, Vancouver, British Columbia, Canada.
[2]Now at Department of Civil and Coastal Engineering, University of Florida, Gainesville, Florida, USA.

0148-0227/09/2008JC004956$09.00

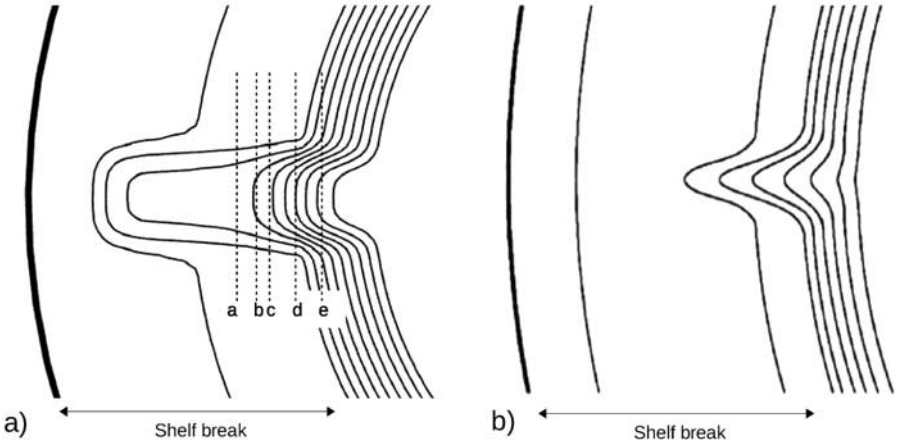

Figure 1. Geometry of the laboratory (a) long and (b) short canyons. Figures 1a and 1b are to the same scale. The short canyon geometry is measured from the physical canyon; the long canyon was built to the plans in Figure 1. Isobaths are 1 cm apart, except the shallowest on the left, which is at 0.5 cm. Lines a, b, c, d, and e denote the position of the cross-sectional light sheet used in conjunction with horizontal layers of fluorescence dye. The distance from the edge of the tank (thick line) to the shelf break is 22.5 cm.

short canyons occur during upwelling favorable wind events which generate a geostrophic incident flow [*Kinsella et al.*, 1987; *Hickey*, 1997]. *Allen* [2000] showed that in a short canyon, higher-order effects generate the flow inside the canyon and no upwelling occurs for strictly geostrophic flow.

[4] The dynamics of long canyons are less well understood. Over long canyons it is possible for upwelling to occur with geostrophic flow in all regions (except at specific singular points [*Allen*, 2000]). Despite several field experiments studying both the wind-response in long canyons [*Carmack and Kulikov*, 1998] as well as various interactions driving upwelling [*Freeland and Denman*, 1982; *Vindeirinho*, 1998], the flow in long canyons and the difference in the flow to that of its shorter counterpart remain relatively unknown.

[5] Our study, based on a laboratory model, will focus on flow in long canyons and how it compares to its short canyon counterpart as well as how changes in velocity and stratification affect the flow dynamics. Thus far, several laboratory experiments involving short canyons have been done [*Pérenne et al.*, 1997, 2001a, 2001b; *Allen et al.*, 2003; *Mirshak and Allen*, 2005] but no laboratory experiments of long canyons have been performed. Understanding and describing the flow dynamics will not only help build on the current understanding of the physics in long canyons but also describe how local flow patterns and biology will be affected by these unique topographic features, in particular, in the regions surrounding Juan de Fuca Canyon.

[6] In this paper, the flow dynamics in long canyons under low Rossby number flow will be evaluated. The experimental methods, including scaling and flow visualization, will be described in the next section. Following this section, the observed flow in the long canyon will be described including a discussion on vorticity generation. Next, a comparison to the observed flow in a short canyon under similar low Rossby number conditions will be made. Last, the results obtained from both the long and short canyon experiments will be classified by considering three possible upwelling mechanisms.

2. Methods

[7] The tank used in this experiment is a circular tank which has a 10-fold vertical exaggeration compared to the depth scale of the ocean. The tank has a gently sloping shelf at 5° (22.5 cm horizontal length from the edge of the tank) followed by a sharply sloping continental shelf of 47° and a 20.5 cm flat abyssal region for a total tank radius of 50 cm. The depth of the tank, when filled, is 10 cm from the surface to the bottom at the tank center with the shelf break depth at 2.2 cm from the surface. Further details of the tank topography can be found in papers by *Allen et al.* [2003] and *Mirshak and Allen* [2005].

[8] Two canyon topographies, a long canyon and a short canyon, are used in this experiment and are built into a 22° slice from the tank topography. The long canyon is a shortened, straightened version of the Juan de Fuca canyon which is rectangular in shape (“u-shaped”), featuring a long separation between the slope of the canyon mouth and the slope of the canyon head. Although the model long canyon does not completely interact with the coast (tank edge), the depth of the continental slope beyond the canyon head is shallow. Results where the depth at the head of the canyon was shallower than in the experiments presented here (approximately 4 mm, 40 m in the real world) were qualitatively similar [*Waterhouse*, 2005]. The short canyon, a smoothed version of Astoria canyon, is more triangular (“v-shaped”) with a uniformly sloping region from the canyon mouth to the head with no separation between the slope at the mouth and head [*Mirshak and Allen*, 2005]. The width of Juan de Fuca canyon and model canyons is large in comparison to the radius of deformation (7.7 km for Juan de Fuca canyon and 3 cm for the model canyons) indicating that these canyons are wide [*Klinck*, 1989; *She and Klinck*, 2000]. The bathymetric contours of both canyons are shown in Figure 1.

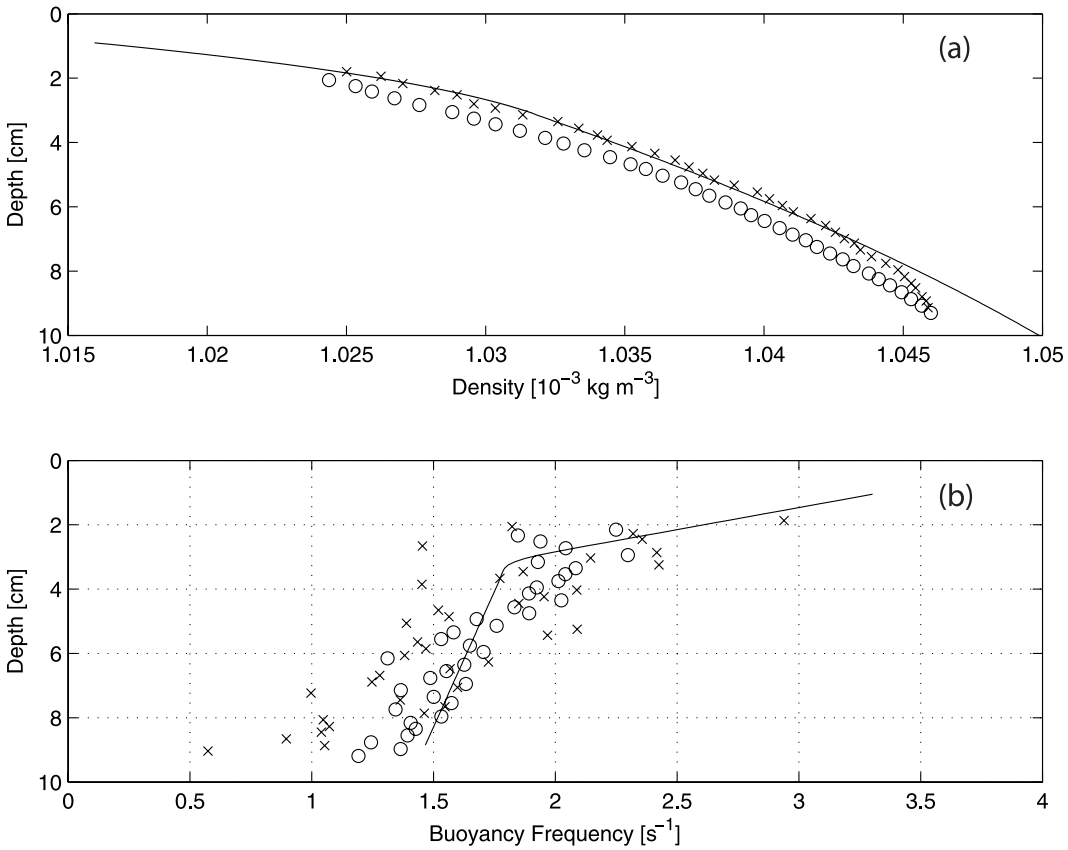

Figure 2. (a) The tank density profile showing the predicted profile as a solid line and the measured profile (crosses and circles). The crosses represent the average values from three separate conductivity probes on the upward profile, while the circles are from the downward profile. (b) The buoyancy frequency in the tank from theory (solid line) and the measured buoyancy frequency (crosses and circles). For purposes of this experiment, the buoyancy frequency at the shelf break level is used in the scaling analysis.

[9] To obtain a realistic density structure in the tank, the *Oster* [1965] two-bucket method is used to fill the tank over a 90-min interval while the tank is rotating [*Mirshak and Allen*, 2005]. The density profile (Figure 2), measured using a microconductivity probe in the nonrotating case, shows a shift of the theoretical and measured density curves. Two possible reasons for this are diffusion, and water column mixing due to the movement of the conductivity probe. Despite the shift of the density profiles in relation to the theoretical curves, the dynamically important variable for appropriate tank scaling is the buoyancy frequency, N, which agrees between experimental and theoretical results within measurement error.

2.1. Scaling

[10] To scale the laboratory model such that it is comparable to the ocean, the following nondimensional numbers are used: (1) the Rossby number ($Ro = U/(f R)$), where U is the velocity, f is the Coriolis parameter (where $f = 2\ \Omega$, where Ω is the rotation rate of the tank), and R is the radius of curvature of the isobaths upstream of the canyon [*Allen et al.*, 2003; *Mirshak and Allen*, 2005]; (2) the Froude number ($Fr = U/(N H_s)$), where N is the buoyancy frequency ($N^2 = -g/\rho\ \Delta\rho/\Delta z$), where g is the gravitational constant, z is the vertical coordinate, ρ is the density, H_s is the depth of the shelf break; and (3) the Burger number ($Bu = N H_s/(f L_c)$), where L_c is the length of the canyon.

[11] The Coriolis parameter, the buoyancy frequency, and the incident velocity are the parameters that will be varied in the lab experiments and therefore will be calculated such that the nondimensional numbers match between Juan de Fuca Canyon and the long canyon–scale version. Table 1 displays the values known for Juan de Fuca Canyon and the corresponding values for the two physical models. Since it is difficult to observe quantifiable changes in the flow at low velocities, f is chosen to be high such that the forcing velocities are high and the Rossby number is low.

2.2. Initiating the Flow

[12] The experimental apparatus rotates at a fixed speed during spin-up, which takes approximately 2 h before solid body rotation is achieved [*Mirshak and Allen*, 2005]. To obtain the required incident velocity, the tank speed is changed from $f = 1.475\ s^{-1}$ to $f = 1.5\ s^{-1}$ over 27.3 s. The time period over which the change in rotation takes place is equal to several inertial periods, which are chosen to resemble a mean, geostrophic flow in the tank slowly changing over several days. To investigate the change in

Table 1. Complete Physical Variables and Nondimensional Numbers for Juan de Fuca Canyon and the Physical Laboratory Model

Physical Variables and Nondimensional Numbers	Symbol	Juan de Fuca	Model Long Canyon	Model Short Canyon
Shelf break depth	H_s	180 m	2.2 cm	2.2 cm
Shelf length	L_s	68.6 km	22.5 cm	22.5 cm
Canyon length	L_c	45 km	16.5 cm	8.0 cm
Canyon width (average)	W	12 km	5.8 cm	3.0 cm
Canyon width (shelf break)	W_{sb}	23 km	6.5 cm	6.0 cm
Radius of curvature of H_s	R	7.7 km	1.4 cm	1.4 cm
Coriolis parameter	f	1.08×10^{-4} s^{-1}	1.5 s^{-1}	1.5 s^{-1}
Buoyancy frequency at H_s	N	4.6×10^{-3} s^{-1} [a]	2.0 s^{-1}	2.0 s^{-1}
Incident velocity	U	10.0 cm s^{-1} [b]	0.3 cm s^{-1}	0.3 cm s^{-1}
Rossby number	Ro	0.12	0.14	0.14
Froude number	Fr	0.12	0.07	0.07
Burger number	Bu	0.17	0.18	0.37
Width ratio	W/W_{sb}	0.52	0.89	0.5
Width-length ratio	W/L_c	0.26	0.35	0.38
Length-length ratio	L_s/L_c	1.52	1.36	2.81

[a]Conductivity-temperature-depth data available from Institute of Ocean Sciences, Station LW7, located at 48°0.05'N, 125°21.97'W from 7 September 2001.
[b]Data from *Freeland and Denman* [1982].

dynamics with velocity and stratification, several experiments are conducted. The corresponding nondimensional numbers and frequencies used are summarized in Table 2.

[13] Initial investigations into the incident flow in the tank show that the flow over the shelf break, in this particular tank, does not follow $u = \Delta\Omega r$ where r is the radius of the tank. The velocity decreases because of the increased friction over the shelf [*Pérenne et al.*, 2001b; *Mirshak and Allen*, 2005]. Therefore, flow just offshore of the shelf will be stronger and faster than flow onshore (along the shelf), each following nearly separate linear relationships (Figure 3).

[14] Because of the nature of the incident flow, the velocity offshore of the shelf break is calculated at 30 and 60 s to verify how the incident offshore velocity changes over the specified time interval. The difference in velocity between the two time intervals (0.002 cm s^{-1}) was well below the measurement error (±0.06 cm s^{-1}). Therefore, the velocity off the shelf does not change significantly over time.

2.3. Flow Visualization

[15] To record the changes in the flow, two basic geometries for the laboratory configuration of the camera and slide projector are used. The first has a video camera centered over the canyon giving a plan view of the canyon area [*Mirshak and Allen*, 2005]. A thin sheet of light is emitted from the slide projector (above the center of the tank) which projects onto a mirror placed in the center of the tank. The reflection from the mirror produces a thinly lit horizontal cross-sectional area inside the canyon between the shelf break depth and less than 1 cm above the shelf break depth. Given that near surface flow is only weakly affected by the canyon [*Hickey*, 1997; *Allen et al.*, 2003], the observation depth from the horizontal light sheet (1.2 to 2.2 cm for the long canyon and 1.9 to 2.2 cm for the short canyon) is sufficient for observing upwelling from the canyon. The second geometry requires switching the position of the video camera and projector giving a vertical cross-sectional view of the canyon from the reflecting mirror positioned in the center of the tank.

[16] Three different flow visualization methods are used in this experiment. The first uses neutrally buoyant particles made from wax and titanium dioxide powder illuminated by horizontal light sheets, either white or multicolored. The particles are mixed with a surfactant and added to the tank approximately 5 min before data collection begins and after spin-up of the tank is complete.

[17] The second visualization method involves the use of fluorescein dye with a vertical plane of light. For these experiments, three common depths for the marked layers are chosen at 5 cm, 7 cm and 8.5 cm, as measured from the surface. As the tank fills, 1 ml of dye solution is injected into the filling hose at the particular depths creating a horizontal layer of dye at each of the prescribed depths. The vertical light sheet is moved farther toward the head of the canyon with each experimental run (lines a through e in Figure 1) to obtain a three-dimensional representation of the flow. Although diffusion occurs between the time of the dye injection and the end of spin-up (resulting in dye layers 0.5 cm thick), the amount of diffusion occurring while the experiment is being run (over 60 s) is negligible compared with other data acquisition and processing errors [*Waterhouse*, 2005].

[18] The third visualization technique involves placing dye-filled syringes directly into the water (both on and below the shelf break) and releasing the dye a set period of time after the initial change in rotations rate (30 s) using a horizontal sheet of light to illuminate the area of interest. This technique is used to observe the effect of upwelling

Table 2. Nondimensional Numbers for Various Chosen Velocities

U (cm s^{-1})	N (s^{-1})	Δf	Ro
0.16	2	0.0125	0.08
0.30	2	0.025	0.14
0.47	0	0.0375	0.24
0.47	1	0.0375	0.24
0.47	2	0.0375	0.24
0.47	3	0.0375	0.24
0.47	3.75	0.0375	0.24
0.60	2	0.048	0.29
1.50	2	0.12	0.71

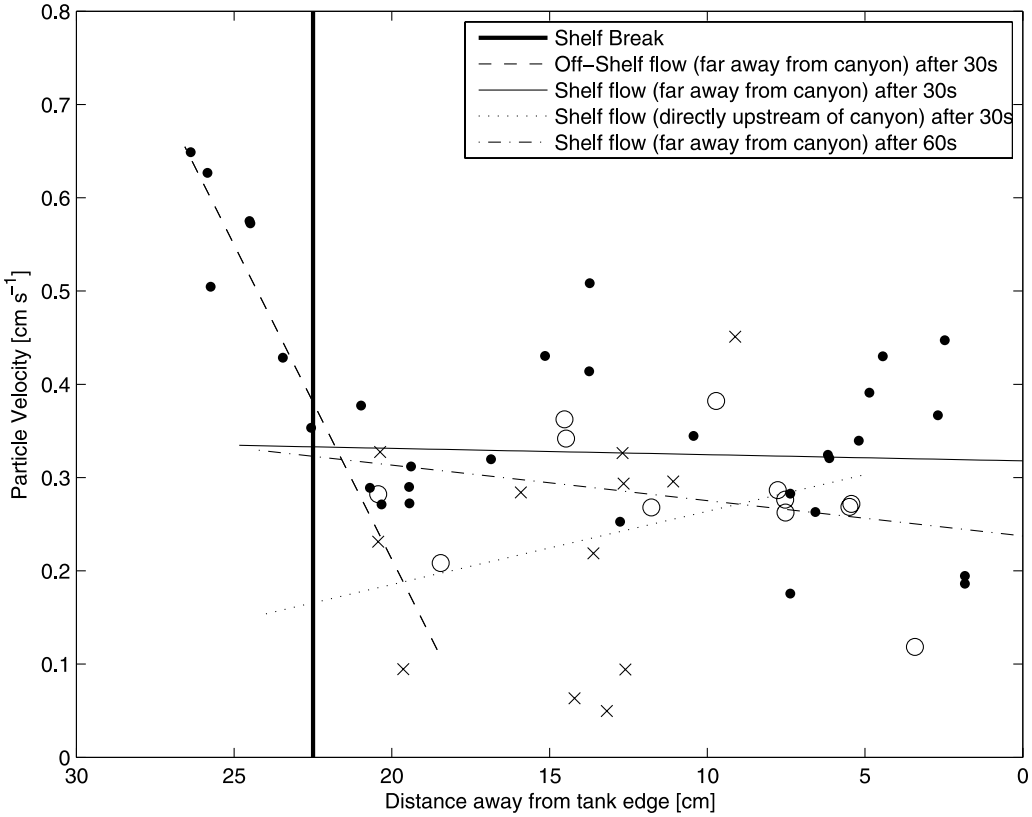

Figure 3. Velocity on the shelf when $U = 0.5$ cm s^{-1}, $N = 2$ s^{-1} far away from the long canyon 30 s after the initial change in rotation rate (solid dots) with fits to the off-shelf flow (dashed line with $U = (0.07 \pm 0.02)$ s^{-1} $r + (-1.1 \pm 0.5)$ cm s^{-1}) and shelf flow (solid line with $U = (0.0007 \pm 0.002)$ s^{-1} $r + (0.32 \pm 0.03)$ cm s^{-1}), upstream of the long canyon 30 s after the initial change in rotation rate (crosses) and the associated fit (dotted line with $U = (-0.008 \pm 0.07)$ s^{-1} $r + (0.3 \pm 0.8)$ cm s^{-1}), and far away from the long canyon 60 s after the initial change in rotation rate (circles) and the associated fit (dotted-dashed line with $U = (0.004 \pm 0.006)$ s^{-1} $r + (0.24 \pm 0.06)$ cm s^{-1}). The vertical line at 22.5 cm represents the location of the shelf break where 0 cm is the tank edge (corresponding with the coastline). Velocity measurements are taken from 0.5 to 2.2 cm depth using a white light sheet.

from below the canyon rim and whether or not upwelling is originating from rim depth or below the rim depth.

2.4. Data Acquisition and Image Analysis

[19] All of the data is collected using a mounted digital video camera recording images at 30 frames per second. Images captured using the multicolored light sheet are processed by tracking individual particles and their respective changes in color 30 s after the initial change in rotation rate. Using the known depths of the colored light sheets for the long canyon (red between 1.2 and 2.2 cm, green between 2.2 and 3.2 cm, and blue between 3.2 and 4.2 cm) and the short canyon (red and white between 2.8 to 2.2 cm and yellow, green and blue between 2.2 to 1.3 cm), vertical as well as horizontal displacements are observed.

[20] Images captured using the white horizontal light sheet are processed by creating particle streak images over a time interval ranging between 2 to 6 s depending on the incident velocity (shorter time interval for faster flow speed). Using these streak images (included in Appendix A) in combination with the video recordings, interpretations of the flow from the captured data are generated (Figure 4). Regions of the topography which do not contain particles are not interpolated and left blank.

[21] For the second visualization method, the images are adjusted to a threshold which allows for the isolation and identification of the top and bottom layer of the dye. The third visualization technique requires no further processing.

3. Results: Long Canyon

[22] The first visualization technique results in vertical and horizontal particle displacements. Upwelling is observed in the multicolored light sheet experiments by displacements of particles from the lower layers to the shelf break depth while the white light sheet experiments give streak pictures of the horizontal velocity field.

[23] The streak images are used for determination of the horizontal velocity field as fewer particles are available from the multicolored light sheet experiments. The drawback in using the streak images is that we cannot directly observe vertical "upwelling" velocities from these streak images. However, for flow near the depth of the topography, flow across the isobaths (from deep to shallow) is expected

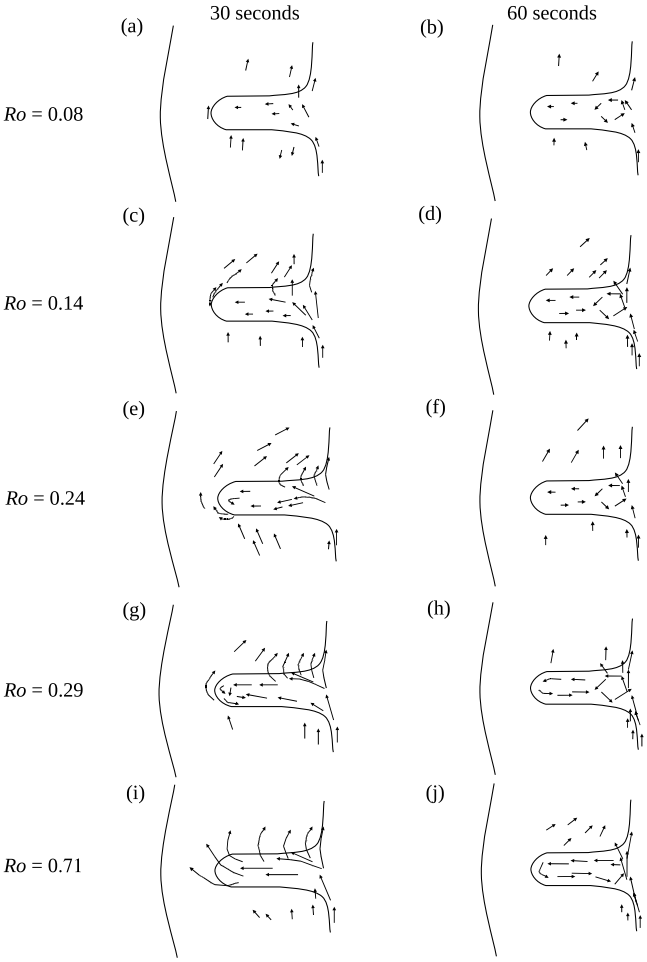

Figure 4. (a–j) Interpretation of the flow in the long canyon for varying Rossby numbers 30 and 60 s after the change in rotation rate of the tank. The shelf break and tank edge are represented by solid black lines, and the flow vectors are representative of the flow between 1.2 and 2.2 cm in the vertical. Arrows are not to scale, but the original data is presented in Appendix A for comparison.

to result in vertical displacements. Our other visualization techniques (multicolored particle tracking after 30 s) and previous observations [*Hickey*, 1997] and models [*Pérenne et al.*, 2001b] show upward flow resulting from such cross-isobath flow. Particles used in the experiment are subject to a small amount of settling. By comparing moving particles upstream of the canyon in the streak images between 30 and 60 s (Figure A1), moving particles observed after 60 s are found at depths deeper than 1.7 cm even though the light sheet is illuminating between 1.2 and 2.2 cm. Therefore, after 60 s, particles that are observed crossing isobaths from within the long canyon are assumed to have vertical displacements associated with this flow. In the short canyon, the flow is observed in a thinner horizontal light sheet (1.9 to 2.2 cm) for the entire duration of the experiments. In the following discussion, we will use the term upwelling when we observe flow from the canyon across the canyon rim, at near rim depths.

3.1. Flow Field at Low Rossby Number

[24] From observations of particle tracks, the flow dynamics at low Rossby number ($Ro = 0.14$) are characterized for two distinct stages of the flow. The two stages are chosen on the basis of the time after the initiation of the impulsively generated flow and the flow at these times are similar within several seconds.

[25] The first and initial stage of the flow, occurring between 30 and 40 s (equivalent to 3.5 to 4.8 days in the real world) after the initial forcing, features the incident velocity acting like a jet along the slope on the upstream side of the canyon (Figure 4c). This flow, between the shelf break and 1 cm above in the vertical, enters the canyon at the mouth upstream of the shelf break and turns into the canyon. When this inflow reaches the downstream wall of the canyon the flow continues toward the canyon head or exits the canyon in the downstream direction. Flow inside the canyon is very slow and begins a slow cyclonic circulation inside the canyon with up-canyon flow along the downstream wall. Cross-isobath flow is observed along the downstream rim of the canyon close to the mouth. On the shelf upstream of the canyon, particles are moving at a diminished speed in the incident flow direction. On the shelf downstream of the canyon, particles are moving downstream and toward the shelf break.

[26] In the second stage of the flow (Figure 4d) when $t >$ 60 s (equivalent to 7 days after the initial forcing), the flow inside the canyon slows. Two well developed cyclonic eddies are visible inside the canyon walls. The first eddy is found just within the canyon mouth (below the rim depth) (Figure 4d). The depth of this eddy goes well below the measurement depths (4 cm or equivalent to 400 m in the oceanic scale). The second eddy is found at the head. Flow on the shelf upstream of the canyon is diminished as was observed at 30 s. Flow downstream of the canyon continues to be directed toward the shelf break. Cross-isobath flow is observed along the downstream rim of the canyon close to the mouth. The summary of the flow at 30 s and 60 s after the initial change in rotation rate are presented in Figure 5.

3.2. Steady State

[27] In an effort to simulate a steady state situation in the laboratory model, the effect of friction on the incident velocity was balanced thus creating a steady current. This was done by continually increasing the rate of rotation of the tank after the initial change, at a new rate of change, $\Delta\Omega_3 = \Delta\Omega_2/\Delta t$. The rate of change required to maintain the desired velocity is achieved by increasing the rotation of the tank from $f = 1.5\ s^{-1}$ to $f = 1.6\ s^{-1}$ over 1000 s (27.3 s after the initial change in rotation rate from $f = 1.4875\ s^{-1}$ to $f = 1.5\ s^{-1}$). Syringes with fluorescein dye were placed upstream of the canyon along the shelf as well as below the shelf break depth on the slope. The light sheet is positioned between 0 and 2.2 cm (i.e., shallower than the shelf break) for full coverage of the shelf break region.

[28] In these steady state experiments, upwelling occurs continuously in the laboratory long canyon for the geostrophic case with $Ro = 0.14$ (Figure 6). Upwelling, from 0.5 cm below the canyon rim depth, occurs on the downstream rim of the canyon close to the mouth in a 4 cm section. A cyclonic eddy is visible trapped inside the canyon mouth and cyclonic circulation is visible in the interior of

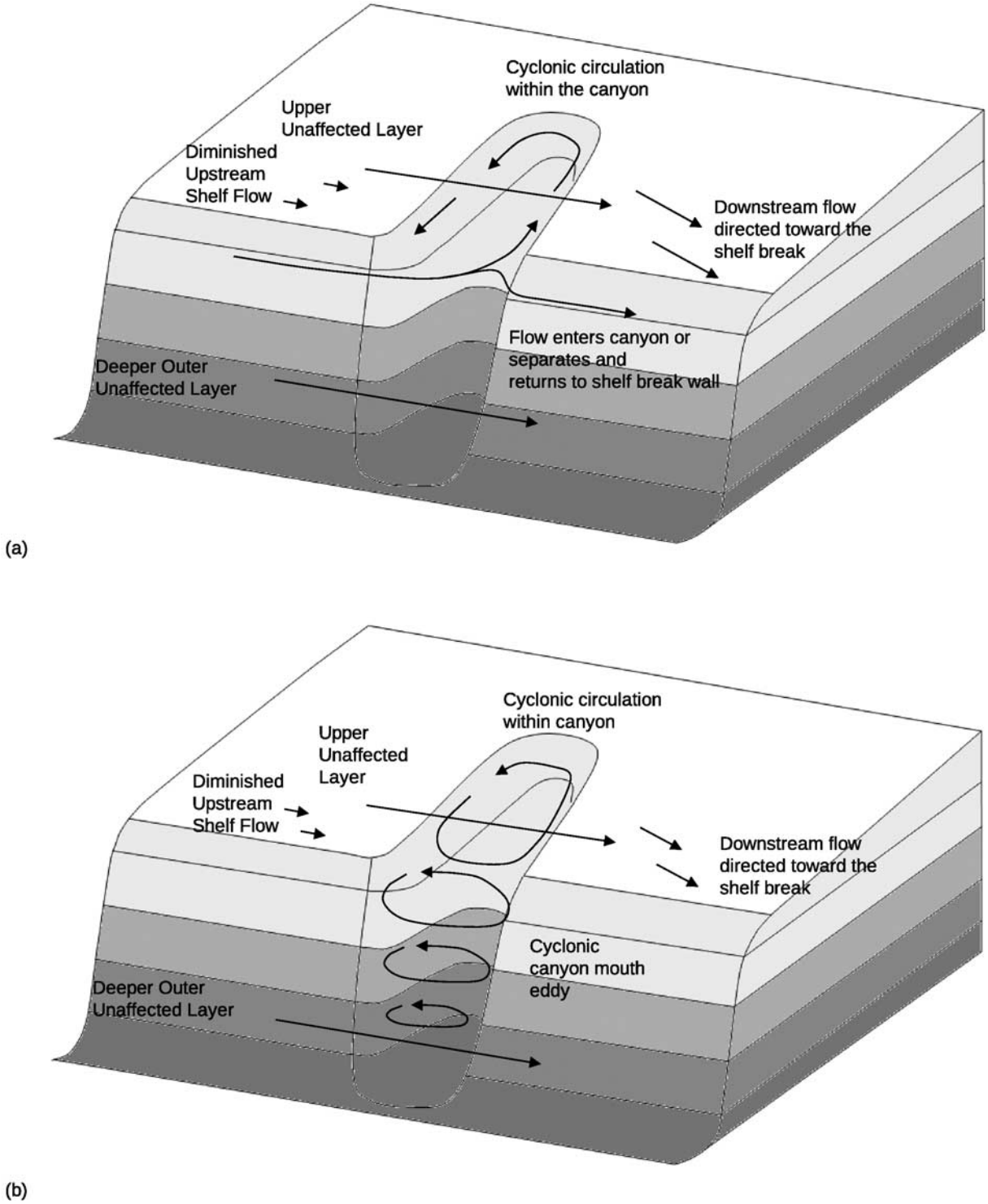

Figure 5. (a) Initial stage of the laboratory flow in the long canyon. Flow separation occurs at the canyon mouth between flow entering the canyon and flow returning along the downstream wall below the shelf break. Flow travels in the offshore direction, below the shelf break depth, and along the upstream wall of the canyon. On the shelf, flow upstream of the canyon is diminished while flow downstream of the canyon is directed toward the shelf break. The flow in the deeper outer layer and upper layer well above the canyon is unaffected. Upwelling occurs close to the mouth along the downstream rim (not shown). (b) Secondary quasi-steady stage of the laboratory flow in the long canyon. Slow cyclonic circulation occurs inside the canyon away from the mouth affecting flow between 2.2 and 4 cm. A small amount of cross-isobath flow (upwelling) occurs close to the canyon mouth (not shown). Flow upstream of the canyon on the shelf is diminished, and the flow in the deeper outer layer and upper layer well above the canyon is unaffected. The shelf break depth is 2.2 cm in Figures 1a and 1b.

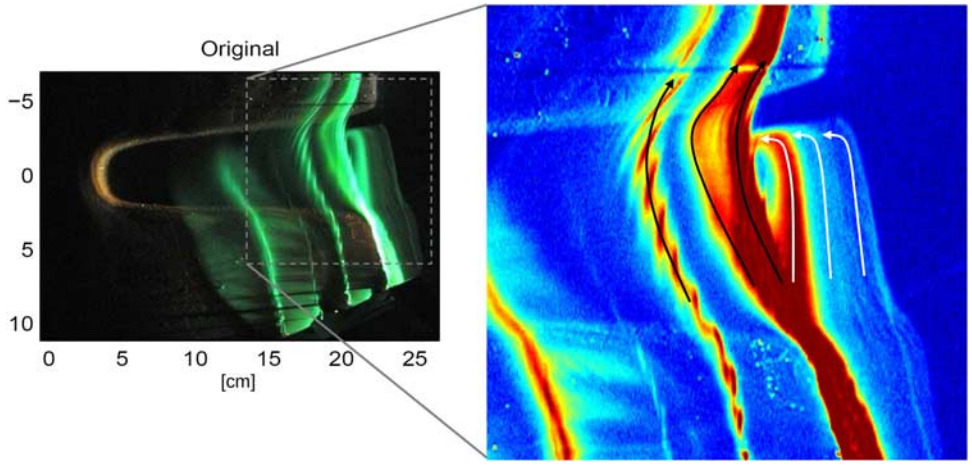

Figure 6. (left) Original and (right) enlargement of the steady state flow at the canyon mouth 200 s after the initial change in rotation rate of the tank. Dye was released from four syringes placed on the shelf upstream of the canyon. The dye released is at the shelf break depth. In the enlargement, red, yellow, and blue indicate high, lower, and zero dye concentrations, respectively. The horizontal light sheet is reflected on the canyon topography, which appears as light blue to yellow. The black and white arrows indicate the flow of the canyon mouth eddy that is observed below the canyon rim depth with the black, and white arrows indicate flow at shallower and deeper depths, respectively. Note the full size of the eddy at the canyon mouth (white arrows) is obscured by the dye above (black arrows).

the canyon up to the canyon head. Flow crosses isobaths along the downstream rim of the canyon close to the mouth. By conservation of volume, as flow crosses isobaths as indicated by the dye (and particles from the previous discussion) moving from deep to shallow areas, upwelling (vertical movement) of water must be occurring to account for the net influx of volume into the system. A flow separation feature is observed at the downstream mouth of the canyon where flow inside the canyon mouth is directed into the canyon via the canyon mouth eddy where it remains in circulation in the eddy or upwells onto the shelf (Figure 6).

3.3. Vorticity

[29] Flow in the canyon contains a significant amount of vorticity which is observed by the formation of a cyclonic eddy at the canyon mouth. The presence of strong vorticity is expected because of the large vertical displacements observed in the water column along the upstream wall of the canyon.

[30] Two possible mechanisms of vorticity generation have been proposed in previous submarine canyon studies: flow separation and vortex stretching [*Pérenne et al.*, 2001b]. From the experiments conducted here, it is proposed that vortex stretching is the most dominant mechanism of in-canyon vorticity generation despite significant shear along the continental slope upstream of the canyon. To determine the influence of each mechanism, we will discuss the affect of stratification on the canyon eddy.

[31] The first possible mechanism of vorticity generation is due to flow separation. As incident alongshore flow meets the downstream canyon wall, flow separation occurs whether the canyon is moderately stratified or highly stratified [*Waterhouse*, 2005]. This process occurs because of incident flow traveling along the slope, which is affected by friction against the slope and as a result, has a strong shear. Once across the canyon mouth, part of the flow detaches from the slope and part of the flow follows the radius of curvature of the tank. Vorticity due to the shear against the slope may initiate cyclonic motion in the flow as it encounters the canyon. In general, there does not appear to be a difference in the relationship between velocity and distance away from the wall as stratification changes (Figure 7) [*Waterhouse*, 2005]. To determine the strength of the vorticity generated because of this shear, a best fit function is found for all of the stratification cases to determine an equation that describes the velocity close to a wall.

[32] The equation describing the velocity on a sloping wall [*Pedlosky*, 1987] as well as the velocity in solid body rotation is fitted to the velocity data using a nonlinear least squares fit and is of the form

$$U = U_{interior} * Boundary\ layer\ correction \tag{1}$$

where U is the velocity of the flow defined by

$$U = \Delta\Omega(r - x)\left(1 - e^{-x/L}\right) \tag{2}$$

where r is the radius of the tank, and x is the variable distance away from the wall. A fit to the experimental data gives $\Delta\Omega = 0.013 \pm 0.001\ s^{-1}$ and $L = 0.4 \pm 0.2$ cm where L is the length scale constant (Figure 7). The error for the fit is calculated using a bootstrap method. As expected, the vorticity closest to the wall is the greatest. However, because of the fact that the velocity is slow very close to the continental slope, the vorticity due to the shear will likely not affect the flow inside the canyon until a long time after the flow has been initiated given how quickly the vorticity decreases away from the shelf slope (Figure 7b).

[33] The second possible mechanism of vorticity generation is due to vortex stretching. Water columns traveling along the continental shelf, originating upstream of the

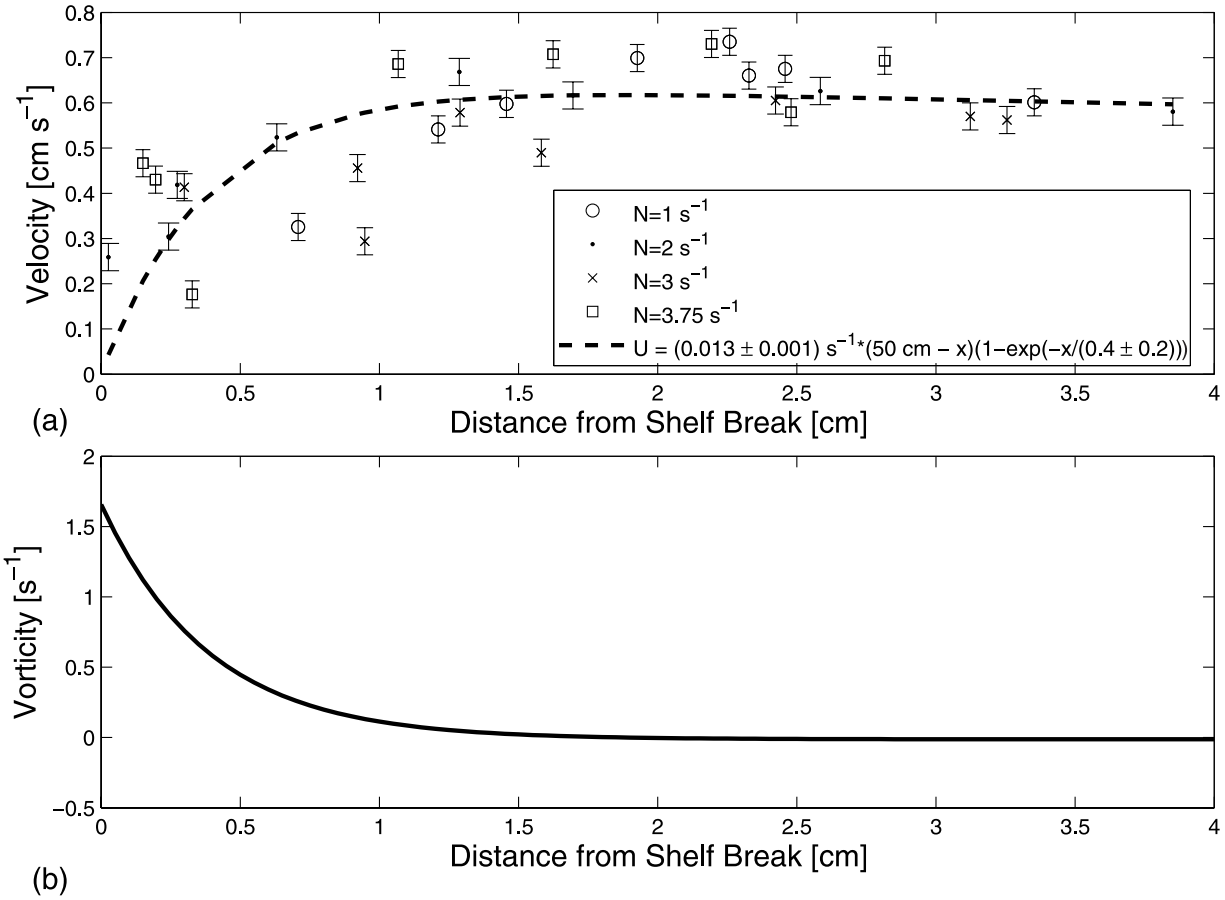

Figure 7. (a) The upstream particle velocity (cm s^{-1}) increases exponentially away from the wall. Results are plotted for various stratifications. There does not appear to be any difference in velocity profile between the different stratifications. (b) The associated vorticity for the fit to the measured velocities from Figure 7a.

canyon, will flow over top of the canyon. As the water columns encounter the canyon, they will stretch as a result of an increase in bottom depth downstream of the upstream canyon rim. The water column stretching, due to conservation of potential vorticity, creates cyclonic vorticity in the flow at the upstream side of the canyon [*Hickey*, 1997]. When stratification is high (and the Burger number is large), stretching of water columns originating from the shelf is more difficult as they fall into the canyon. In a highly stratified fluid, parcels from the shelf will maintain their vertical level because of the large amount of energy required to drop into the canyon and stretch. When the water column does not stretch, there will be less generation of cyclonic vorticity in the canyon. Conversely, if the Burger number is lower, a water parcel encountering the canyon will more easily drop into the canyon generating more cyclonic vorticity because of vortex stretching.

[34] Changes in the thickness of the dye in the vicinity of the long canyon for low Rossby number (Ro = 0.14) were quantitatively measured by using the second visualization method. The vertical light sheet was set up at five different locations (lines a–e in Figure 1). As an example, the evolution of the dye layer at position c is shown in Figure 8. Although upwelling is not observed in the displacement of the dye layer below the shelf break, the tilted nature of the dye corresponds with observations of tilted isopycnals below the canyon rim [*Hickey*, 1997]. The results of observed vertical displacements of the dye divided by the initial thickness of the dye are expressed as stretching (positive value) or compression (negative value) in f-units (Table 3).

[35] This analysis shows that the greatest amount of stretching occurs on the upstream side of the canyon from Positions c–e on the scale of 0.2–0.5f over 60 s. The difference in stretching between the upstream location and the other locations varies from 5 to 12 times. From conservation of potential vorticity, the large amount of stretching at the upstream side of the canyon will induce a cyclonic vorticity. Stretching increases along the upstream wall of the canyon as the measurement location moves closer to the canyon head (from a to d in Table 3). There is a smaller amount of stretching midcanyon as well as along the downstream canyon wall (except for at location d).

[36] If isopycnal stretching were solely responsible for vorticity generation, the vorticity of the canyon mouth eddy will increase linearly with inverse stratification. Using (2), the vorticity due to shear generation between 0.5 to 2 cm away from the wall ranges between 0.45 to 0 s^{-1} which is

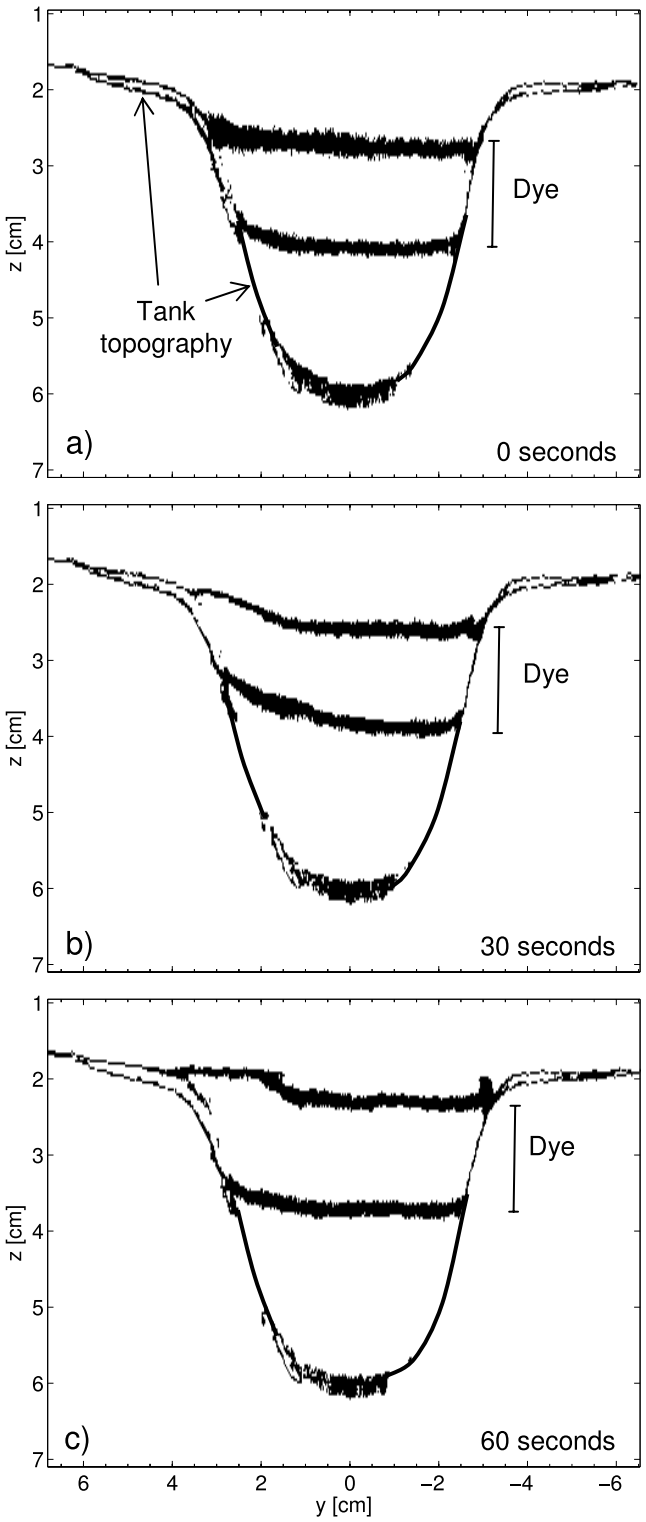

Figure 8. Evolution of the horizontal layer of dye (vertical light sheet at position c) at (a) 0 s, (b) 30 s, and (c) 60 s after the initial change in rotation rate of the tank. The top and bottom bounds of the dye are indicated. Flow is directed from left to right, and view is toward the head of the canyon from the ocean (middle of the tank).

not insignificant; however, vorticity follows a linear relationship with inverse stratification such that

$$\zeta = \frac{p}{N} - q \tag{3}$$

where the coefficients $p = (0.4 \pm 0.2)\ s^{-2}$ and $q = (0.05 \pm 0.08)\ s^{-1}$ and the error corresponds to the 95% confidence interval. The intercept is close to zero which indicates that when stratification is infinite, no (or very little) vorticity will be observed, within error of the fit (Figure 9). If sidewall friction was significant to vorticity generation inside the canyon, the intercept of the fit would be positive indicating that with no stretching, vorticity will still occur. Therefore, even through frictional shear is large far away from the shelf break, velocity close to the shelf slope is too small to account for the observed vorticity within the canyon. Vorticity in the canyon is, primarily, generated via vortex stretching since frictional shear will not have enough inertia to enter the canyon.

4. Comparison: Long and Short Canyons

[37] As Rossby number increases, flow features in the long and short canyons show both similarities and differences that are more easily compared using both the multicolored and white light sheet experiments.

[38] The tracked multicolored particles in the long and short canyons show differing patterns of upwelling (Figure 10). In the long canyon, upwelling occurs very close to the canyon mouth after 30 s as only one particle is observed moving from below the shelf break (green) to above the shelf break depth (red in Figure 10a). Particles within the canyon are moving in the cyclonic direction at the mouth as well as midway through the canyon as discussed in section 3.1. In the short canyon, upwelling occurs more predominantly along the entire downstream rim for a similar forcing velocity as well as through the canyon head with movement of four particles from below the shelf break (red and white) to above the shelf break depth (yellow, green and blue in Figure 10b). Only one particle is observed moving offshore inside the canyon along the upstream side.

[39] The particle streak images also show differences in the horizontal pattern of upwelling and flow dynamics between the long and short canyons (Figures 4 and 11). The key flow features will be summarized below for each Rossby number and are separated into two separate cases: 30 s and 60 s after the initial change in rotation rate.

[40] At large Rossby number (Ro = 0.71), the long canyon acts like a short canyon in that upwelling (cross-isobath flow) occurs in both canyons after 30 s along the entire downstream rim of the canyon as well as though the canyon head. After 30 s, no canyon mouth eddy is observed in either long or short canyons. Flow on the shelf upstream of the canyon is diminished by the long canyon (Figures 3 and 4) but not affected by the short canyon. After 60 s, the canyon mouth eddy exists in both long and short canyons. The interior canyon flow shows similar features between the long and short canyons. The interior canyon flow at high Rossby number has one large cyclonic eddy, an effective canyon mouth eddy in both cases, which encompasses the entire length and width of both long and short canyons. A

Table 3. Stretching and Compression of the Horizontal Dye Layers[a]

Position	Upstream	Midcanyon	Downstream
a	0.01 ± 0.03	0.01 ± 0.02	0.00 ± 0.02
b	0.11 ± 0.01	0.07 ± 0.01	0.03 ± 0.01
c	0.21 ± 0.01	−0.02 ± 0.01	0.03 ± 0.01
d	0.49 ± 0.03	−0.02 ± 0.02	−0.09 ± 0.01
e	0.23 ± 0.01[b]	0.12 ± 0.01	0.45 ± 0.01[b]

[a]Expressed in f-units, over 60 s of the time series. Upstream, midcanyon, downstream represent the position from the center of the canyon axis (−1.5 cm, 0 cm, and 1.5 cm, respectively) across the captured images from the dye experiments. Positions a–e represent the location of the light sheet as shown in Figure 1a.

[b]Results calculated using the difference between the top and middle of the dye layer, not the top and bottom slopes as with the other cases. This is required as the dye in these two cases reaches the topography.

small amount of upwelling (cross-isobath flow) occurs along the downstream wall in the long canyon and the short canyon.

[41] For Rossby numbers lower than 0.71, the flow in the interior of the canyon after the first 30 s acts similarly in both the long and short canyons in that flow is heading toward the canyon head increasing in strength with increasing Rossby number and there is no observed canyon mouth eddy. In the short canyon, the vertical shear is large at medium Rossby number (0.24), with a much smaller shear observed in the long canyon (visible in raw data in Figure A2). The difference in velocity shear between the two canyons, and a larger Hogg scale (fL/N) in the long canyon, indicates that the effects of the long canyon are more barotropic than for a short canyon in that forcing effects reach shallower depths [*Hogg*, 1973]. There is also an observed spilt between flow upwelling onto the shelf on the downstream canyon rim and flow that is traveling toward the canyon head in both canyons. A noticeable change in width of the incoming flow occurs in both canyon lengths with the maximum entrance width occurring at a Rossby number of 0.24. Flow downstream of the canyon is similar in both long and short canyons after both 30 and 60 s with flow being directed toward the shelf break with increasing velocity as Rossby number increases.

[42] Upwelling, in the short canyon, occurs in all cases through the canyon head at 30 s. At Ro = 0.08, flow is traveling onshore along the upstream rim of the canyon and offshore along the downstream rim of the canyon while the flow in all other cases is traveling to the canyon head across the width of the canyon. After 60 s, while upwelling continues to occur in the long canyon, upwelling only occurs through the head and along the downstream rim of the canyon at Ro = 0.71 and only along the downstream rim close to the mouth (not through the head) for Ro = 0.29. Upwelling may be occurring in the short canyon for lower Rossby number flow but because of a scarcity of particles near the head of the canyon after 60 s, cross-isobath flow is not visible.

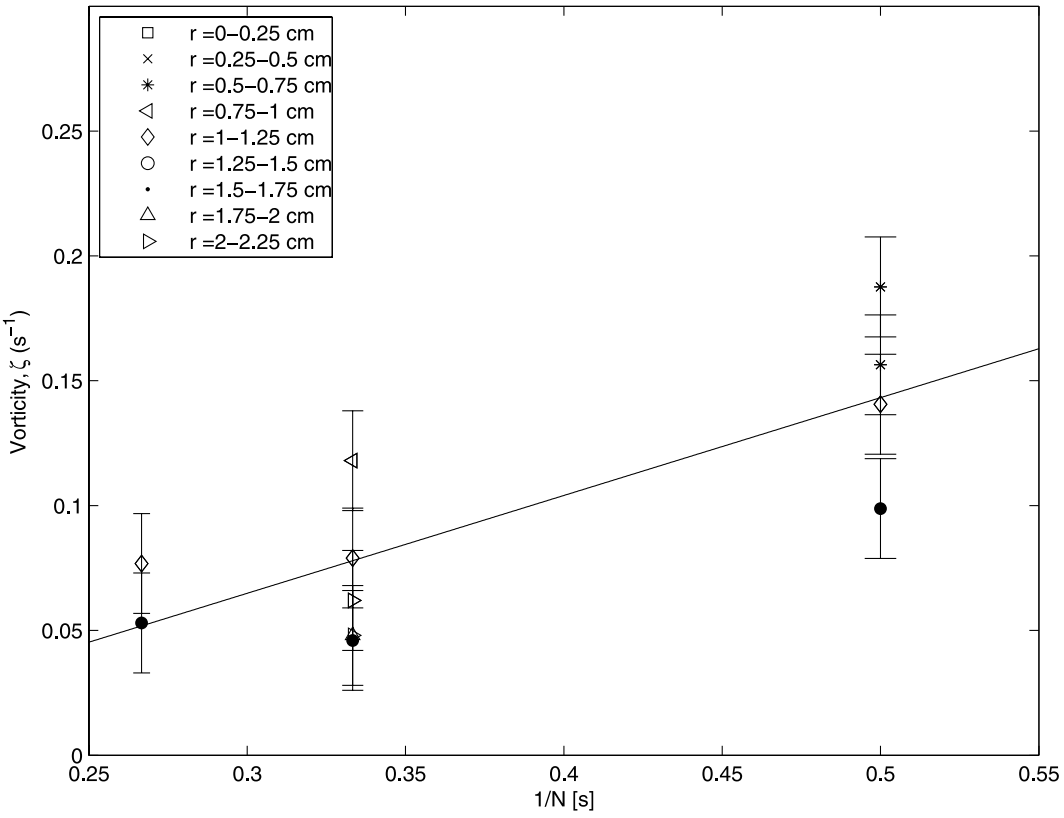

Figure 9. Vorticity of canyon mouth eddy, ζ (s^{-1}), increases with the inverse of buoyancy frequency (N^{-1} (s)) which is indicated by the fit ($\zeta = 0.4 \pm 0.2\ s^{-2}\ N^{-1} - 0.04 \pm 0.08\ s^{-1}$, where the errors in the fit correspond to the 95% confidence intervals). The different symbols represent the radius away from the center of the eddy. The measurement error of the vorticity is 0.02 s^{-1}, and the error of the radius is 0.1 cm. The vorticity increases toward the center of the eddy.

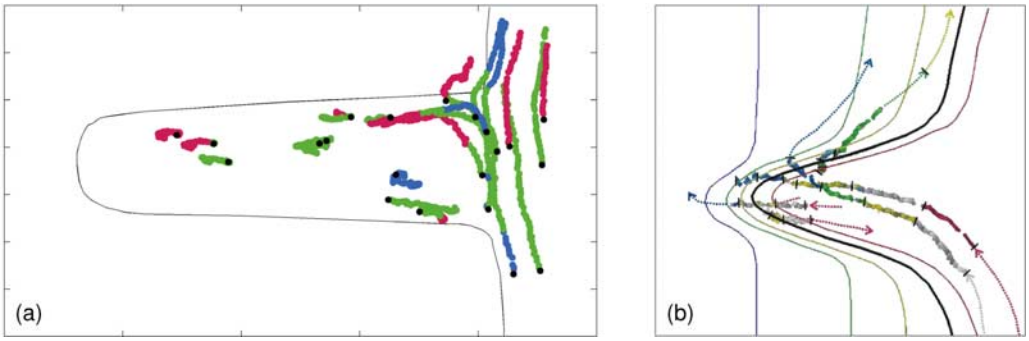

Figure 10. Particle tracking from horizontal multicolored light sheet experiments for the (a) long canyon and (b) short canyon at Ro = 0.24. In Figure 10a, the initial particle location is denoted with a black circle, and red corresponds to above the shelf break (1.2–2.2 cm depth), while green and blue are below the shelf break (2.2–3.2 cm and 3.2–4.2 cm depth, respectively). The image dimensions are 25 × 14 cm. In Figure 10b, the blue, green, and yellow particles are above the shelf break (1.3–1.6 cm, 1.6–1.9 cm, and 1.9–2.2 cm, respectively), while white and red particles are below the shelf break (2.2–2.5 and 2.5–2.8 cm, respectively). The image dimensions are 19 × 13 cm. The shelf break depth (2.2 cm) is denoted by a thick solid black line in Figure 10a and 10b. The ambient flow is traveling toward the top of Figure 10.

[43] A special feature is observed, unique to the long canyon, at both 30 and 60 s after the change in rotation rate. The flow on the shelf, upstream of the canyon, is reduced (in velocity) with the long canyon. This is not observed in the short canyon experiments. At the lowest Rossby number, the flow upstream of the canyon rim, close to the shelf break, is actually observed moving in the upstream direction (Figure 4a). As Rossby number increases, the flow at this location is moving in the downstream direction at a diminished velocity compared to the shelf velocity downstream of the canyon (Figures 3 and 4). Comparing relative streak lengths within Figure A1 (or their representations in Figure 4), we see that velocities are slower on the shelf upstream of the canyon than downstream in all cases. At 60 s, diminished flow on the shelf near the canyon rim is observed, but because of a lack of data at higher Rossby numbers (Ro = 0.29 and 0.71) conclusion can be made only at the three lowest Rossby numbers (Figure 4). In the short canyon after 60 s, the flow upstream of the canyon is of a similar magnitude to the flow downstream of the canyon except for the lowest except for the lowest Rossby number.

5. Discussion

[44] As described in the previous section, there are differences in the flow dynamics between the laboratory long and short canyons. The possible mechanisms driving upwelling in these different dynamical regimes: isobath convergence, advection and time dependence are described below and will be characterized on the basis of their strength as calculated by the respective Rossby number describing the flow.

5.1. Isobath Convergence

[45] Theoretical work has suggested that long canyons, which closely approach the coast, have strongly converging isobaths and should thus exhibit upwelling at quite small Rossby number [*Allen*, 2000]. In particular, specifying the width of the group of converging isobaths as W_T, a topographic scale, gives that the flow cannot follow the topography if

$$C > (Ro_c)^{-0.5} \tag{4}$$

where C is the ratio of the horizontal distance between isobaths far upstream of the canyon (dx_u) to the distance between the isobaths of maximum convergence (dx_c) and the convergence Rossby number is defined by $Ro_c = U/f\,W_T$ where U is the shelf break flow speed. For the two canyons considered here, the width of the canyon at the shelf break, W_{sb}, is a good measure of the total width of converging isobaths.

[46] It was expected that canyons would have significant upwelling at low Rossby Number in regions where isopycnals strongly converged. In the theoretical canyon [*Allen*, 2000], this feature occurred at the head of the canyon, but here, for the long canyon, it occurs from midway along the sides of the canyon (Figure 1). The isobath experiencing the maximum convergence value is 1.7 cm depth, about 2 cm coastward of the shelf break giving C = 24. This is the region where upwelling over the rim is observed (Figure 12a). If the mechanism of *Allen* [2000] is at work, one would expect that upstream of the canyon, the flow along the ''converged'' isobaths would be weak or ''blocked'' as weak total flux for these isobaths is transmitted upstream from the canyon by shelf waves. Observations show that flow in this region just upstream of the canyon is about 50% as strong as flow farther upstream at the same depth (Figures 3 and 11).

[47] Comparatively, there is no clear evidence of blocking upstream of the short canyon in that flow on the shelf upstream of the canyon, flows in the downstream direction at the same speed as flow farther upstream (Figures 11 and A2). Convergence of isobaths is considerably weaker in the short canyon topography not only because of the fact it is shorter but also because of the more triangular shape. Maximum convergence occurs near the head at about 1.5–2 cm depth giving C = 5. This convergence is below

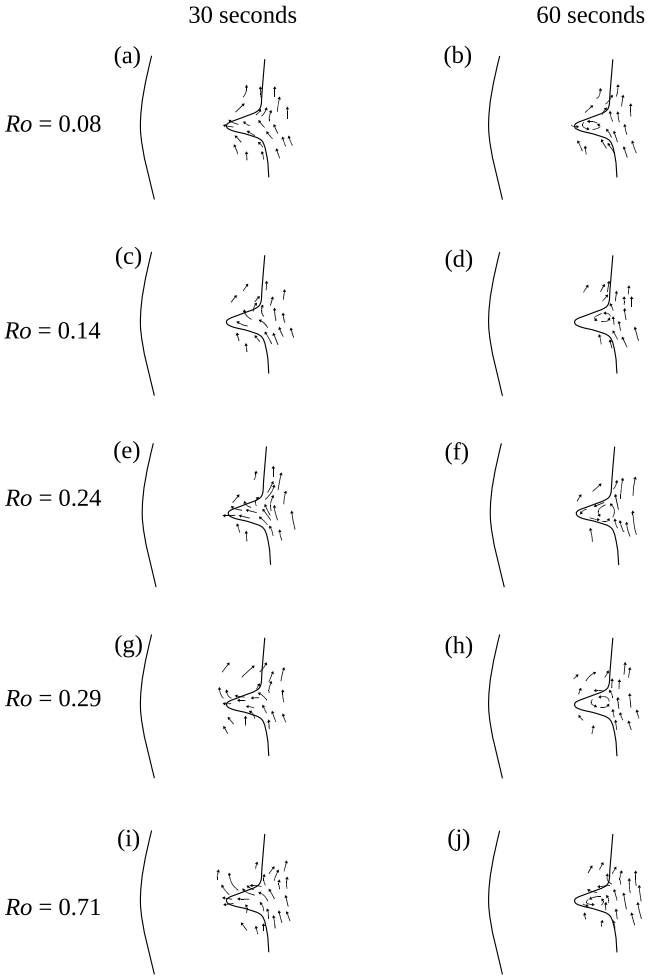

Figure 11. (a–j) Interpretation of the flow in the short canyon for varying Rossby numbers 30 and 60 s after the change in rotation rate of the tank. The shelf break and tank edge are represented by solid black lines, and the flow vectors are representative of the flow between 1.9 and 2.2 cm in the vertical. Arrows are not to scale, but the original data is presented in Appendix A for comparison.

the range of convergences expected to cause some upstream "blocking."

5.2. Advection

[48] At larger Rossby numbers, flow is no longer geostrophic in regions beyond those where isobaths converge. At these Rossby numbers, upwelling caused by flow crossing the canyon because of advection is expected to dominate. Results from the laboratory short canyon at the highest Rossby number in the first stages of the flow show this advective upwelling regime which has been observed in both field data [*Hickey*, 1997] and laboratory experiments [*Allen et al.*, 2001; *Pérenne et al.*, 2001a, 2001b; *Mirshak and Allen*, 2005]. In this work, the criteria for determining the strength and importance of the advective regime in driving upwelling is through the advective Rossby number ($Ro = U/fR$). If the advective Rossby number is greater than 0.2 (Tables 4 and 5), this mechanism is important and drives flow characterized by upwelling at the canyon head with no blocking of the flow on the upstream side of the canyon (Figure 12b). Note, that actual velocities have been calculated in Tables 4 and 5 to take into account the effect of friction described in Figure 3 and section 2.2. From this point on, the Rossby numbers calculated using the actual velocities will be used.

[49] Upwelling in the short canyon occurs (and is visible) between an advective Rossby number of 0.1 to 0.52 during the first 30 s by the advective mechanism. Both the time-dependent and isobath convergent criteria are low in comparison (Table 4). After 60 s, upwelling through the head of the canyon is not visible in the short canyon except for an advective Rossby number of 0.50 and again, time-dependent and isobath convergent criteria are low, in comparison (Table 5). At $Ro = 0.20$, upwelling is observed near the mouth of the canyon and although it is not observed at the head of the canyon, the advective Rossby number is

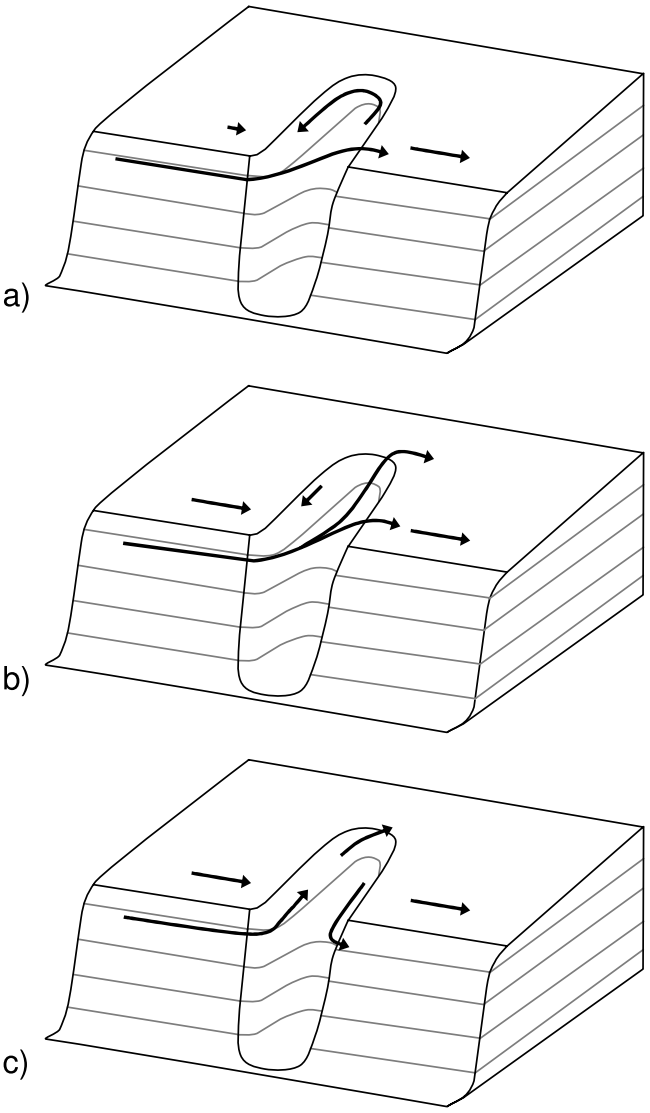

Figure 12. Flow schematic of three upwelling mechanisms: (a) isobath convergence, (b) advection, and (c) time dependence of the flow.

Table 4. Nondimensional Rossby Numbers (Time-Dependent (Ro_t), Advective (Ro), and Convergent (Ro_c)) for Long and Short Laboratory Canyons[a]

Forcing Velocity (cm s^{-1})	Actual Shelf Velocity (cm s^{-1})	Time-Dependent		Advective	Isobath Convergence		Upwelling Observed	Dominant Mechanism	Upwelling Flow Shown in
		$Ro_t = 1/f\,t$	Criteria (5) > 0.25	($Ro = U/(f\,R)$; Criteria $Ro > 0.2$)	$Ro_c = U/(f\,W_{sb})$	Criteria From (4) $Ro_c\,C^2 > 1$			
Long Canyon									
0.16	0.12	0.02	0.22	0.06	0.01	6.8[b]	Yes	IC	Figure 12a
0.3	0.22	0.02	0.22	0.1	0.02	12.8[b]	Yes	IC	Figure 12a
0.47	0.34	0.02	0.22	0.16	0.03	20.1[b]	Yes	IC	Figure 12a
0.6	0.43	0.02	0.22	0.21[b]	0.04	25.6[b]	Yes	IC	Figure 12a
1.5	1.09	0.02	0.22	0.52[b]	0.11	64.1[b]	Yes	AD	Figure 12b
Short Canyon									
0.16	0.12	0.02	0.09	0.06	0.01	0.3	Yes	TD	Figure 12c
0.3	0.22	0.02	0.09	0.1	0.02	0.6	Yes	AD	Figure 12b
0.47	0.34	0.02	0.09	0.16	0.04	0.9	Yes	AD	Figure 12b
0.6	0.43	0.02	0.09	0.21[b]	0.05	1.2[b]	Yes	AD	Figure 12b
1.5	1.09	0.02	0.09	0.52[b]	0.12	2.9[b]	Yes	AD	Figure 12b

[a]Rossby number–specific criteria for upwelling occur given the flow regime 30 s after flow initialization. Actual shelf velocities are calculated using results from Figure 3 for shelf velocities measured far away from the canyon. IC, isobath convergence; AD, advective; TD, time-dependent.
[b]Rossby numbers exceed the specified upwelling criteria.

significant compared with the time-dependent and isobath convergence criteria (Table 5). After a long period of time has elapsed, upwelling in a short canyon may continue to occur but will be difficult to visualize from observations in the horizontal flow field as the flow is dominated by the canyon mouth eddy [*She and Klinck*, 2000]. Therefore, although upwelling is not visible in the short canyon 60 s after the flow initialization for lower Rossby number, upwelling may be occurring (''Not visible'' in Table 5).

[50] At the highest Rossby number, the flow in the long canyon also acts in this advective regime at both 30 and 60 s after the flow initiation. As the advective Rossby number decreases, the dynamics in the long canyon are dominated by the isobath convergence regime as the isobath convergence criteria remains high (Tables 4 and 5). This regime continues to show visible upwelling over a longer period of time than the advective regime. Long canyon experiments carried out at a steady state reveal the weak but continuing upwelling due to isobath convergence.

5.3. Time Dependence

[51] With the lowest incident velocity in the short canyon, the flow during the first 30 s shows onshore flow along the upstream side of the canyon and offshore flow along the downstream side, as described above. Given this difference in flow structure, the mechanism responsible for driving this flow and the associated upwelling is related to a time dependence of the flow (Figure 12c).

[52] This third regime, not defined by either advective or isobath convergent processes, is related to the time-dependent changes in flow characteristics defined as the time-dependent Rossby number, $Ro_t = 1/(ft)$ where t is the time after the change in rotation rate of the tank [*Boyer et al.*, 2004]. For time-dependent upwelling to be clearly visible we would expect

$$Ro_t \frac{L_c}{W_{sb}}\left(\frac{W}{a}+2\right) > 0.25 \tag{5}$$

Table 5. Nondimensional Rossby Numbers (Time-Dependent (Ro_t), Advective (Ro), and Convergent (Ro_c)) for Long and Short Laboratory Canyons[a]

Forcing Velocity (cm s^{-1})	Actual Shelf Velocity (cm s^{-1})	Time-Dependent		Advective	Isobath Convergence		Upwelling Observed	Dominant Mechanism	Upwelling Flow Shown in
		$Ro_t = 1/ft$	Criteria (5) > 0.5	($Ro = U/(f\,R)$; Criteria $Ro > 0.2$)	$Ro_c = U/(f\,W_{sb})$	Criteria From (4) $Ro_c\,C^2 > 1$			
Long Canyon									
0.16	0.11	0	0	0.05	0.01	6.6[b]	Yes	IC	Figure 12a
0.3	0.21	0	0	0.10	0.02	12.4[b]	Yes	IC	Figure 12a
0.47	0.33	0	0	0.16	0.03	19.5[b]	Yes	IC	Figure 12a
0.6	0.42	0	0	0.20[b]	0.04	24.9[b]	Yes	IC	Figure 12a
1.5	1.05	0	0	0.50[b]	0.11	62.2[b]	Yes	AD	Figure 12b
Short Canyon									
0.16	0.11	0	0	0.05	0.01	0.3	Not visible	-	-
0.3	0.21	0	0	0.10	0.02	0.6	Not visible	-	-
0.47	0.33	0	0	0.16	0.04	0.9	Not visible	-	-
0.6	0.42	0	0	0.20[b]	0.05	1.2[b]	Yes	AD	Figure 12b
1.5	1.05	0	0	0.50[b]	0.12	2.9[b]	Yes	AD	Figure 12b

[a]Rossby number-specific criteria for upwelling to occur given the flow regime 60 s after flow initialization. Actual shelf velocities are calculated using results from Figure 3 for shelf velocities measured far away from the canyon.
[b]Rossby numbers exceed the specified upwelling criteria.

where L_c is the length of the canyon, W is the canyon width midway between the mouth and head and a is the Rossby radius of deformation (relevant derivation in Appendix B).

[53] For both long and short canyons, this value is weak compared with advective and isobath-convergent criteria except for the incident velocity of 0.15 cm s^{-1}. For the short canyon, flow inside the canyon at this incident velocity is moving toward the head of the canyon along the upstream side during the first 30 s which is indicative of time-dependent flow [*She and Klinck*, 2000] (Tables 4 and 5). Given the small advective and isobath convergent Rossby number criteria (0.06 and 0.3 respectively), the time dependence of the flow, although small, is the dominant mechanism in determining the flow structure. In the long canyon at this small incident velocity, the stronger isobath convergence upwelling is dominating over the advective or time-dependent upwelling regimes, thus time-dependent upwelling may be occurring in the long canyon at this incident velocity but it is most likely masked by the more dominant isobath convergent mechanism.

[54] In summary, the mechanisms driving upwelling in both long and short canyons can be defined by three distinct processes: advection, time dependence of the flow and the effect of isobath convergence. By specifying criteria to determine the strength of each process, the dominant process is determined at both 30 s and 60 s after the initiation of the flow. The long canyon is most strongly affected by the effects of its bathymetry and thus isobath convergence is the most dominant mechanism driving upwelling, with advection becoming important only with strong incident velocities. Upwelling in the short canyon occurs through advective and time-dependent processes.

6. Summary

[55] At low Rossby number, the flow dynamics in the long canyon show two distinct stages of flow that are characterized by separate and distinct features due to the restrictions of isobath convergence within the canyon. The first stage includes the generation of vorticity due to isopycnal stretching inside the canyon on the upstream side, upwelling occurring at the downstream rim at the mouth, a slow cyclonic flow within the canyon walls and a slowing of flow on the shelf upstream of the canyon. The second stage of the flow is characterized by the formation of a canyon mouth eddy and the continuation of the slow cyclonic flow within the canyon walls and again, upwelling occurring at the downstream rim at the mouth. The canyon mouth eddy is found to have a vorticity dependent on stratification while the upstream slope flow is not dependent on stratification. At moderate Rossby number, upwelling in the steady state experiment occurs continuously along the downstream rim of the long canyon driven by isobath convergence processes.

[56] The pattern of upwelling, between the long and short canyons, is different for moderate Rossby number flow with upwelling occurring at the mouth of the long canyon and through the head and downstream rim for the short canyon. At high Rossby number, the long canyon has similar features as the flow in the short canyon in an advective regime with upwelling occurring at the canyon heads in both cases (Figure 12b). In the short canyon, as the Rossby number decreases, upwelling occurs during the first stage of the flow but is not visible during the second stage. Flow (and upwelling) within the short canyon at the lowest Rossby number is likely dominated by the time dependence of the flow (Figure 12c).

[57] In short canyons, upwelling is observed during strengthening flows and high Rossby number flows. Long canyons, such as Juan de Fuca Canyon, however, will have significant upwelling even during quasi-steady, low Rossby number conditions because of isobath convergence.

Appendix A

[58] Figures 4 and 11 are interpretations of the flow observed in the tank on the basis of streak images Figures A1 and A2 as discussed in section 2.3. The actual streak images are presented here for determining the relative changes in the flow speeds (scale) and particle density for each experiment. Original video recordings were used to verify and add to all observations made from these streak images.

Appendix B

[59] The criteria for determining when the temporal Rossby number is of importance depends on the amount of upwelling flux occurring in the time-dependent sense. We can estimate the ratio of up-canyon velocity due to time-dependent effects to the incoming velocity by estimating the flux needed to create a pressure gradient strong enough to turn the incoming velocity around the canyon [*Allen*, 1996]. From geostrophy, the higher pressure over the canyon needed to turn the incoming flow, U, is

$$fU = \frac{1}{\rho}\frac{\partial p}{\partial x}. \tag{B1}$$

From the hydrostatic approximation,

$$\frac{\partial p}{\partial z} = -\rho' g \tag{B2}$$

which is approximately equal to

$$\frac{\partial p}{\partial z} = \rho_0 N^2 \beta \tag{B3}$$

where β is the vertical distance over which the isopycnals need to be lifted to turn the incoming flow. Using (B3) in (B1) and approximating dx as the Rossby radius of deformation, $a = (NH_S)/f$, and dz as H_s, (B1) becomes

$$\beta = \frac{fUa}{N^2 H_s}. \tag{B4}$$

which also gives the rate of change of β to be

$$\frac{\partial \beta}{\partial t} = \frac{fa}{N^2 H_s}\frac{\partial U}{\partial t}. \tag{B5}$$

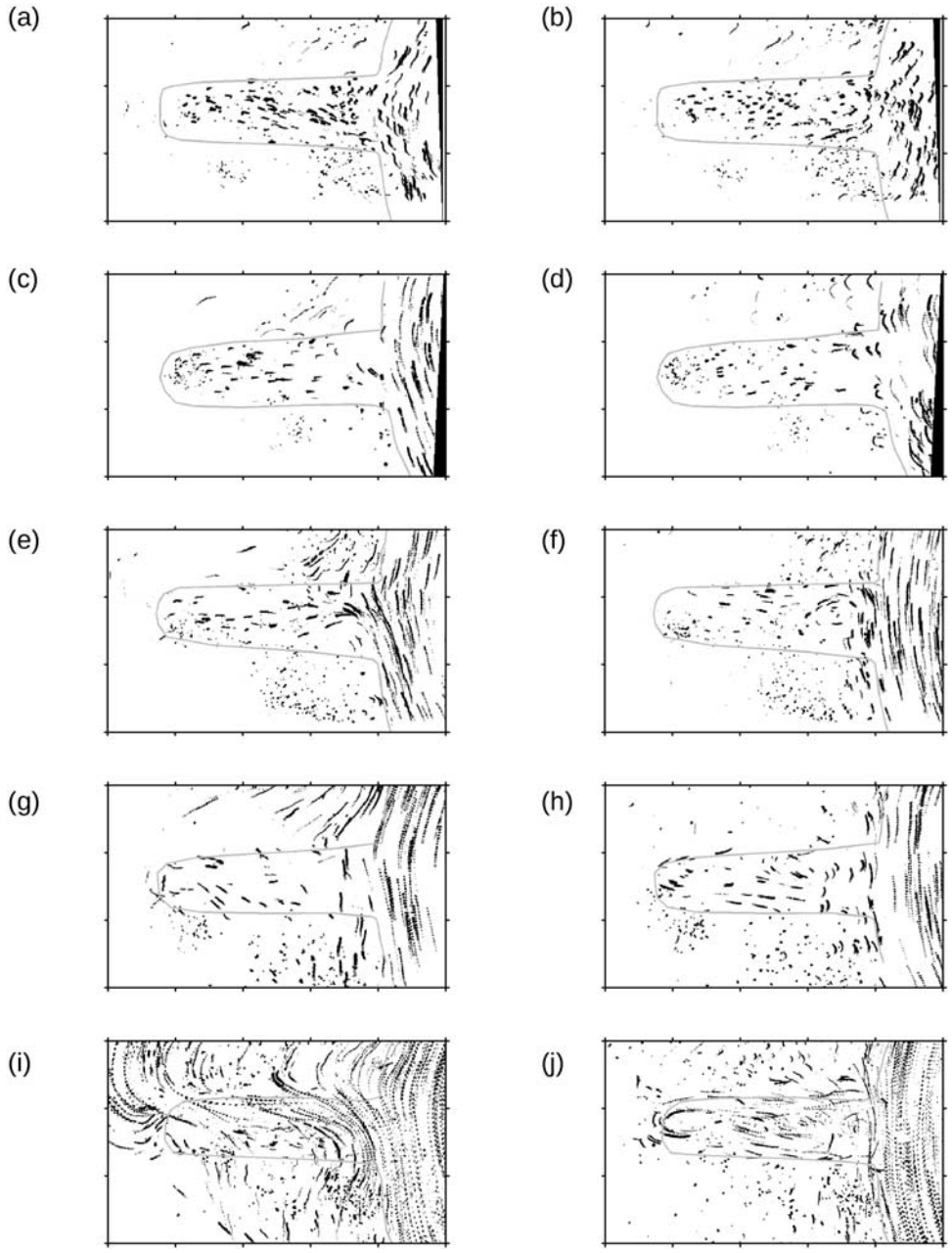

Figure A1. (a–j) Streak images of particle displacement in the long canyon for varying Rossby numbers 30 and 60 s after the initial change in rotation rate of the tank. The shelf break is represented by a solid black line. Observed particles are between 1.2 and 2.2 cm in the vertical. Initial particle locations are denoted by gray streaks, while the particle displacement is captured over 3 s for Figures A1 and A2. Interpretations of the streaks are in Figure 4. Figure A1 dimensions are 25 × 15 cm.

[60] The isopycnals need to be raised through a surface area of the canyon at the shelf break defined by the width of the canyon plus a Rossby radius on either side ($W + 2a$) and the length of the canyon, L_c. This volume is supplied by the up-canyon velocity, multiplied by the width of the canyon at the mouth (W_{sb}) and the prescribed depth of the incoming flow (H_S), to give, approximately

$$U_{upcanyon} W_{sb} H_s = \frac{fa}{N^2 H_s} \frac{\partial U}{\partial t} (W + 2a) L_c \qquad \text{(B6)}$$

which gives an estimate for the up-canyon flow of

$$U_{upcanyon} = \frac{L_c}{f W_{sb}} \frac{\partial U}{\partial t} \left(\frac{W}{a} + 2 \right). \qquad \text{(B7)}$$

[61] Comparing the temporal Rossby number and up-canyon velocity to the velocity of the incoming (cross-canyon) flow, described by $\partial U/\partial t \cdot t$ where t is the time after the initial change in rotation rate of the tank, gives a measure of the strength of the time-dependent flow through the canyon. If the up-canyon flow is at least 25% of the cross-canyon time-dependent flow, then time-dependent

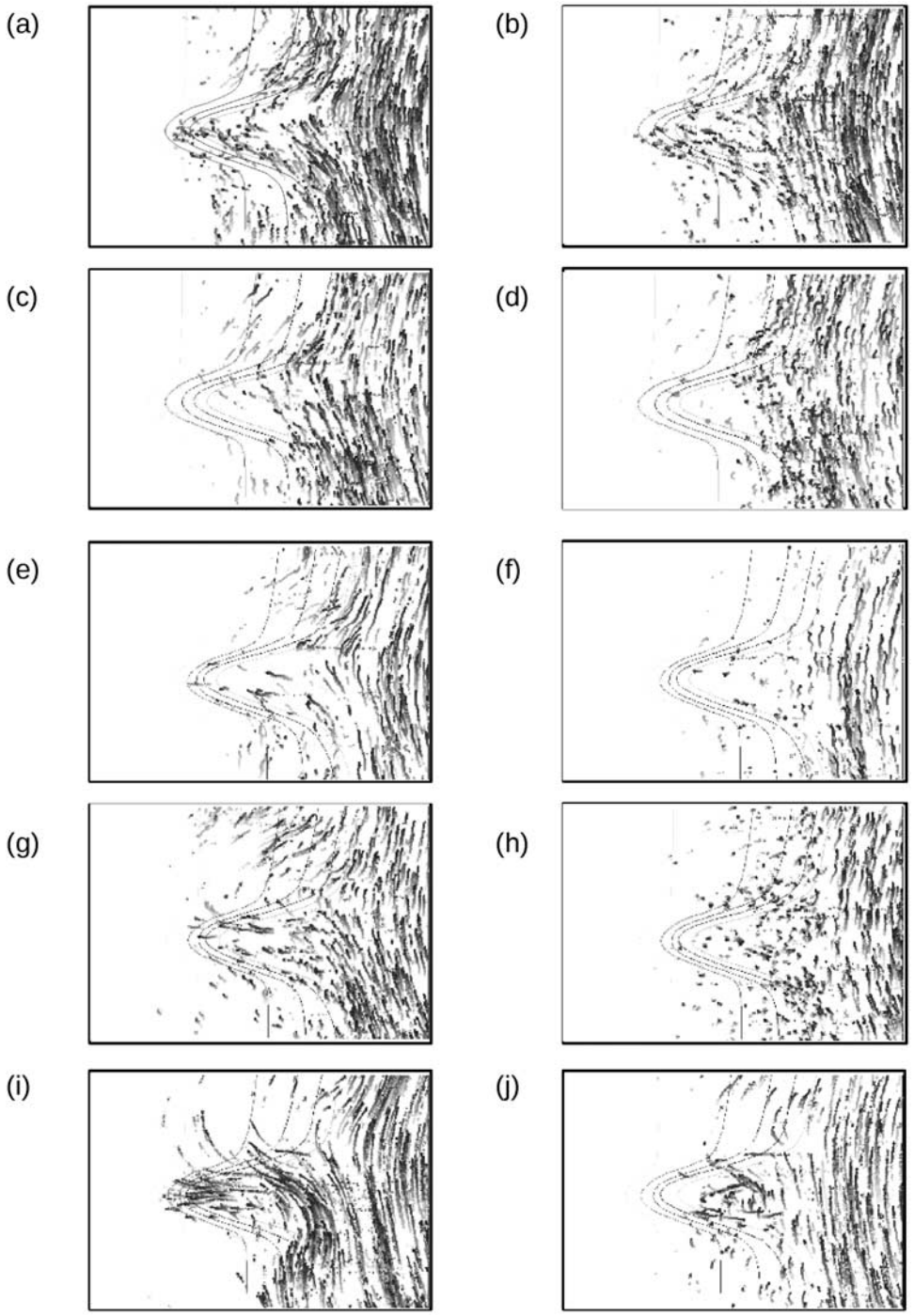

Figure A2. (a–j) Streak images of particle displacement in the short canyon for varying Rossby numbers 30 and 60 s after the initial change in rotation rate of the tank. Streaks are captured over 8 s in Figures A2a and A2b; 4 s in Figures A2c, A2d, A2e, and A2f; and 2 s in Figures A2g, A2h, A2i, and A2j. The canyon contours are represented by solid black lines. Interpretations of the streaks between 1.9 and 2.2 cm depth are in Figure 11. Figure A2 dimensions are 19 × 13 cm.

canyon upwelling should be visible. This gives the following criteria for the time dependence upwelling of the flow

$$Ro_t \frac{L_c}{W_{sb}} \left(\frac{W}{a} + 2 \right) > 0.25. \quad \text{(B8)}$$

[62] **Acknowledgments.** The authors would like to acknowledge Harald Schrempp, Ted Tedford, and Christian Reuten for their technical assistance in the laboratory work and data analysis. The comments of John Klinck and an anonymous reviewer substantially improved the clarity of the paper. This research was supported by an NSERC Discovery grant to the second author.

References

Allen, S. E. (1996), Topographically generated, subinertial flows within a finite length canyon, *J. Phys. Oceanogr.*, *26*, 1608–1632, doi:10.1175/1520-0485(1996)026<1608:TGSFWA>2.0.CO;2.

Allen, S. E. (2000), On subinertial flow in submarine canyons: Effect of geometry, *J. Geophys. Res.*, *105*, 1285–1297, doi:10.1029/1999JC900240.

Allen, S. E., C. Vindeirinho, R. E. Thomson, M. G. G. Foreman, and D. L. Mackas (2001), Physical and biological processes over a submarine canyon during an upwelling event, *Can. J. Fish. Aquat. Sci.*, *58*(4), 671–684, doi:10.1139/cjfas-58-4-671.

Allen, S. E., M. S. Dinniman, J. M. Klinck, D. D. Gorby, A. J. Hewett, and B. M. Hickey (2003), On vertical advection truncation errors in terrain-following numerical models: Comparison to a laboratory model for upwelling over submarine canyons, *J. Geophys. Res.*, *108*(C1), 3003, doi:10.1029/2001JC000978.

Boyer, D. L., D. B. Haidvogel, and N. Pérenne (2004), Laboratory-numerical model comparisons of canyon flows: A parameter study, *J. Phys. Oceanogr.*, *34*, 1588–1609, doi:10.1175/1520-0485(2004)034<1588:LMCOCF>2.0.CO;2.

Carmack, E. C., and E. A. Kulikov (1998), Wind-forced upwelling and internal Kelvin wave generation in Mackenzie Canyon, Beaufort Sea, *J. Geophys. Res.*, *103*, 18,447–18,458.

Freeland, H., and K. Denman (1982), A topographically controlled upwelling center off Vancouver Island, *J. Mar. Res.*, *40*, 1069–1093.

Hickey, B. M. (1997), The response of a steep-sided narrow canyon to time-variable wind forcing, *J. Phys. Oceanogr.*, *27*, 697–726, doi:10.1175/1520-0485(1997)027<0697:TROASS>2.0.CO;2.

Hogg, N. G. (1973), On the stratified Taylor column, *J. Fluid Mech.*, *58*(3), 517–537, doi:10.1017/S0022112073002302.

Kinsella, E. D., A. E. Hay, and W. W. Denner (1987), Wind and topographic effects on the Labrador Current at Carson Canyon, *J. Geophys. Res.*, *92*, 10,853–10,869, doi:10.1029/JC092iC10p10853.

Klinck, J. M. (1989), Geostrophic adjustment over submarine canyons, *J. Geophys. Res.*, *94*, 6133–6144.

Kunze, E., L. K. Rosenfeld, G. S. Carter, and M. C. Gregg (2002), Internal waves in Monterey submarine canyon, *J. Phys. Oceanogr.*, *32*, 1890–1913, doi:10.1175/1520-0485(2002)032<1890:IWIMSC>2.0.CO;2.

Macquart-Moulin, C., and G. Patriti (1996), Accumulation of migratory micronekton crustaceans over the upper slope and submarine canyons of the Northwestern Mediterranean, *Deep Sea Res., Part I*, *43*, 579–601, doi:10.1016/0967-0637(96)00039-8.

Mirshak, R., and S. Allen (2005), Spin-up and the effects of a submarine canyon: Applications to upwelling in Astoria Canyon, *J. Geophys. Res.*, *110*, C02013, doi:10.1029/2004JC002578.

Oster, G. (1965), Density gradients, *Sci. Am.*, *213*, 70–76.

Pedlosky, J. (1987), *Geophysical Fluid Dynamics*, 2nd ed., Springer, Ann Arbor, Mich.

Pérenne, N. P., J. Verron, D. Renouard, D. L. Boyer, and X. Zhang (1997), Rectified barotropic flow over a submarine canyon, *J. Phys. Oceanogr.*, *27*, 1868–1893, doi:10.1175/1520-0485(1997)027<1868:RBFOAS>2.0.CO;2.

Pérenne, N. P., D. B. Haidvogel, and D. L. Boyer (2001a), Laboratory-numerical model comparisons of flow over a coastal canyon, *J. Atmos. Oceanic Technol.*, *18*, 235–255, doi:10.1175/1520-0426(2001)018<0235:LNMCOF>2.0.CO;2.

Pérenne, N. P., J. W. Lavelle, and D. L. Boyer (2001b), Impulsively started flow in a submarine canyon: Comparisons of results from laboratory and numerical models, *J. Atmos. Oceanic Technol.*, *18*, 1698–1717, doi:10.1175/1520-0426(2001)018<1699:ISFIAS>2.0.CO;2.

She, J., and J. M. Klinck (2000), Flow near submarine canyons driven by constant winds, *J. Geophys. Res.*, *105*, 28,671–28,694, doi:10.1029/2000JC900126.

Vindeirinho, C. (1998), Currents, water properties and zooplankton distribution over a submarine canyon under upwelling-favorable conditions, MS thesis, Univ. of B. C., Vancouver, B. C.

Waterhouse, A. F. (2005), A physical study of upwelling flow dynamics in long canyons, MS thesis, Univ. of B. C., Vancouver, B. C.

S. E. Allen and A. W. Bowie, Department of Earth and Ocean Sciences, University of British Columbia, Vancouver, BC V6T 1Z4, Canada.

A. F. Waterhouse (corresponding author), Department of Civil and Coastal Engineering, University of Florida, Gainesville, FL 32611, USA. (awaterhouse@ufl.edu)